Structure and Madelung energy of spherical Coulomb crystals

R. W. Hasse
ESR Division, Gesellschaft für Schwerionenforschung GSI, D-6100 Darmstadt, Germany

V. V. Avilov
ESR Division, Gesellschaft für Schwerionenforschung GSI, D-6100 Darmstadt, Germany and L.D. Landau Institute for Theoretical Physics, SU-117334 Moscow, U.S.S.R.

(Received 26 March 1991)

With the help of molecular-dynamics computer simulations, we study the equilibrium configurations of systems of N =2–5000 strongly correlated charged particles under the influence of a radial harmonic external confining force and their mutual Coulomb forces. The temperature is well below the crystallization point; i.e., the ratio of Coulomb to kinetic energy is as large as $\Gamma = 10^9$. The particles arrange in concentric spherical shells with approximately constant intershell distances. On the surfaces plane hexagonal structures are well pronounced. The calculated radii, occupation numbers, and energies per particle are compared with results of classical geometrical and shell models with homogeneously charged shells corrected for hexagonal surface occupation. The closed-shell particle numbers also agree well with those of multilayer icosahedra. From the computer simulations we extract a Madelung (excess) energy of −0.8926, which is close to the theoretical value of the shell model corrected for plane hexagonal surfaces, −0.8923, but larger than the one of the infinite geometrical lattice, −0.8944, and of the bcc value of −0.8959. Surface-energy effects are positive and of the order of $N^{-1/3}$.

PACS number(s): 32.80.Pj, 52.25.−b, 52.65.+z, 52.75.Di

I. INTRODUCTION

The experimental verification of Coulomb crystals in magnetic traps [1–5] stimulated the continuation of theoretical research on the finite one-component plasma (OCP) at very low temperature. Whereas the structure and thermodynamics of infinite Coulomb matter have been studied extensively, for a review see Ref. [6], the two-dimensional calculations of Thomson [7] were long the only information available on finite systems. These studies were followed by calculations and computer simulations on the structure of cylindrical systems [8, 9], on two- and three-dimensional spherical and spheroidal systems [10–16] with the most recent systematic study of the structure of small systems by Rafac *et al.* [17], on the slab geometry [18], and by realistic calculations in a Paul trap [19].

The essential information gained from these studies is that a strongly correlated infinite OCP crystallizes in a bcc lattice if the plasma parameter, i.e., the ratio of Coulomb to thermal energy, reaches the value [20] $\Gamma \approx 171$. Furthermore, finite systems exhibit *hexagonal* structures on the surfaces, however imperfect, due to the incompatibility between a perfect lattice and a curved surface and due to the incommensurability of two adjacent shells. A change of structure (in the case of slabs) from the *plane hexagonal* into the bcc one occurs only if the dimensions of the system become as large as about 100 interparticle distances.

The energetics of finite systems, however, has not been studied in detail. Apart from results on cylindrical structures [16], on small spherical systems [17] and on slabs [18] systematic calculations on other finite systems, in particular on large spherical systems, are not available. It is the main purpose of this paper to calculate the Madelung energies of small to large spherical Coulomb crystals and to study the lattice structure and its geometry. Here any realistic calculation must reach very low temperatures corresponding to plasma parameters well above the crystallization point. Since the relative energy difference of two different structures, which have the same number of particles and which are both close to the absolute energy minimum, is of the order of 10^{-5}, plasma parameters of 10^5, for very large systems up to 10^9, must be reached.

We employ the molecular-dynamics (MD) technique and calculate the equilibrium configurations of systems of 2 to 5000 particles and control the kinetic energy by reducing the momenta. After the system has settled into up to 11 shells with clearly visible hexagonal lattices the results are analyzed according to their total, single-shell, and rms radii, the shell occupation numbers, and their Madelung energies, i.e., the difference in energy per particle of the MD system and the equivalent homogeneous system. These results then are compared to results of simple geometrical and onion-shell models where the different shells consist of layers of homogeneously charged spheres with the energy corrected for hexagonal surface occupation. The MD computer simulations are presented in Sec. II, and in Secs. III–VI the homogeneous, geometrical, and shell models and their limits for large particle numbers are developed and the results are compared with each other.

II. MOLECULAR DYNAMICS

The infinite OCP is neutralized by an oppositely charged background. An N-particle finite Coulomb crystal, on the other hand, is bound by an external harmonic confining force acting on particle i,

$$\mathbf{F}^i_{\rm conf} = -K\mathbf{r}_i \ , \tag{1}$$

which, at equilibrium and zero kinetic energy, cancels the Coulomb forces of all other particles of charge q in the interior,

$$\mathbf{F}^i_{\rm Coul} = -q^2 \sum_{j\neq i} \frac{\mathbf{r}_i - \mathbf{r}_j}{|\mathbf{r}_i - \mathbf{r}_j|^3} \ . \tag{2}$$

In the outside region, however, there remains an effective binding force. The classical equations of motion

$$m\ddot{\mathbf{r}}_i = \mathbf{F}^i_{\rm conf} + \mathbf{F}^i_{\rm Coul} \quad ({\rm i}=1,\ldots,{\rm N}) \tag{3}$$

are solved numerically with given initial coordinates and velocities. The latter are chosen at random so as to give an initial kinetic energy corresponding to $\Gamma \approx 1$. The initial coordinates of N ions usually are chosen as those of the (N–1)-ion system with one ion added at random, thus reducing computer time as compared to an initial random system, because only one ion has to find its place in the lattice with the other $N-1$ particles only moving slightly. The system is then followed in time until thermal equilibrium has been reached. Then the momenta are reduced (usually by a factor of 10) and the procedure is repeated until the desired Γ value has been reached. For small systems $N \leq 60$ even the expected final structure was taken as the initial configuration and the different final energies were analyzed according to the absolute minimum, thus assuring that for $N \leq 60$ the minimum energy structures had been found. For $N > 60$ this need not always be the case. This is different from the method of Ref. [17], where many random initial conditions were used. An additional check of whether the final structure has reached equilibrium is provided by the fact that for spherical systems the Coulomb energy of the system is equal to twice the confining energy [14]. Systems with $N = 2, 3, 4$ simply are calculated analytically.

In the following, distances (radii) will be measured in units of the Wigner-Seitz radius

$$a_{\rm WS} = \left(\frac{q^2}{K}\right)^{1/3} \tag{4}$$

and energies in units of $q^2/a_{\rm WS} = (q^4K)^{1/3}$. The confining and Coulomb energies per particle then become

$$\varepsilon_{\rm conf} = \frac{1}{2N}\sum_{i=1}^{N} \mathbf{r}_i^2 \ , \tag{5}$$

$$\varepsilon_{\rm Coul} = \frac{1}{N}\sum_i \sum_{j\ (<i)} |\mathbf{r}_i - \mathbf{r}_j|^{-1} \ , \tag{6}$$

and the total energy per particle is just the sum of both.

The results are listed in Table I together with the rms radii, the energy per particle, and the Γ value aimed at. For the small systems $N \leq 27$, they agree with those of Ref. [17]; in particular, that the second shell starts at N=13. In addition, the third shell starts at N=61, and the next ones at or around N=147, 309, 565, 900, 1400, and 2100, respectively. These magic numbers are equal or close to those of the multilayer icosahedra of Mackay [21],

$$N = 1 + \sum_{\nu=1}^{M}(10\nu^2 + 2) \ , \tag{7}$$

which recently were found in alkali-metal clusters [22]. The magic icosahedra particle numbers are listed in Table II and for large N the number of shells becomes

$$M = \left(\frac{3}{10}N\right)^{1/3} - \frac{1}{2} \ . \tag{8}$$

The subshell numbers here are given by $10N^2 + 2$ and can also be found partially in Table I.

Even at the high values of Γ indicated, the particles in the inner shells of large systems have more kinetic energy than those in the outer shells because in the interior the confining potential is very weak, thus washing out the inner shells. An exact analysis of the inner shells, hence, is not posssible. The largest system analyzed with 5000 particles has at least 11 shells.

An *infinite* Coulomb system can take advantage of all long-range interactions in order to arrange in a bcc lattice and to minimize the Madelung energy by summing up all long-range contributions. A *finite* system, on the other hand, can explore only the short- and intermediate-range

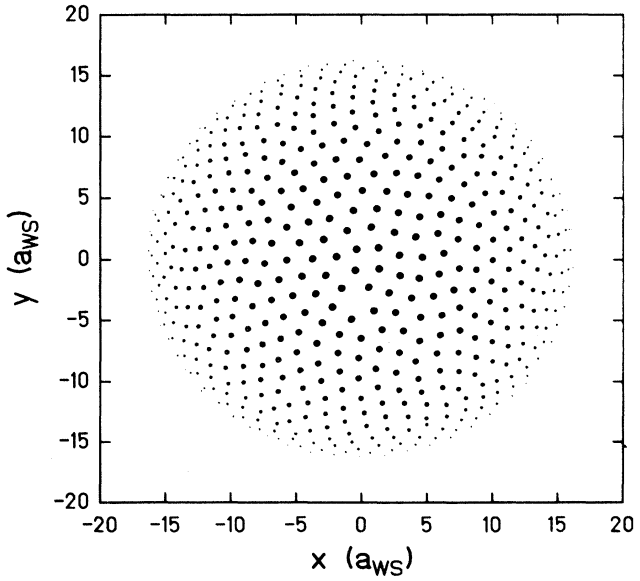

FIG. 1. The front hemisphere of the outer shell of the 5000-ion system. Note the haxagonal structure with approximately equilateral triangles and the point defect below the center.

TABLE I. Structures ($N_M + N_{M-1} + \cdots + N_1$ particles in subshells), rms radii, and energies of N-particle systems.

N	Structure	$R_{\rm rms}$	ϵ	Γ
2	2	0.6300	0.5953	∞[a]
3	3	0.8327	1.0400	∞[a]
4	4	0.9721	1.4174	∞[a]
5	5	1.0901	1.7820	10^5
6	6	1.1850	2.1065	10^5
7	7	1.2736	2.4321	10^5
8	8	1.3500	2.7331	10^5
9	9	1.4198	3.0238	10^5
10	10	1.4846	3.3058	10^5
11	11	1.5453	3.5822	10^5
12	12	1.6002	3.8407	10^5
13	12+1	1.6535	4.1009	10^5
14	13+1	1.7036	4.3542	10^5
15	14+1	1.7508	4.5972	10^5
16	15+1	1.7956	4.8364	10^5
17	16+1	1.8387	5.0707	10^5
18	17+1	1.8852	5.3010	10^5
19	18+1	1.9197	5.5275	10^5
20	19+1	1.9583	5.7521	10^5
21	20+1	1.9947	5.9705	10^5
22	21+1	2.0311	6.1873	10^5
23	21+2	2.0657	6.4001	10^5
24	22+2	2.0990	6.6090	10^5
25	23+2	2.1318	6.8166	10^5
26	24+2	2.1633	7.0197	10^5
27	24+3	2.1941	7.2206	10^5
28	24+4	2.2241	7.4200	10^5
29	26+3	2.2532	7.6162	10^5
30	27+3	2.2818	7.8098	10^5
31	28+3	2.3098	8.0026	10^5
32	28+4	2.3368	8.1900	10^5
33	29+4	2.3635	8.3788	10^5
34	30+4	2.3895	8.5648	10^5
35	30+5	2.4150	8.7488	10^5
36	30+6	2.4401	8.9307	10^5
37	31+6	2.4646	9.1107	10^5
38	32+6	2.4885	9.2887	10^5
39	33+6	2.5123	9.4676	10^5
40	34+6	2.5356	9.6437	10^5
41	35+6	2.5585	9.8187	10^5
42	35+7	2.5810	9.9921	10^5
43	36+7	2.6031	10.1638	10^5
44	37+7	2.6222	10.3342	10^5
45	38+7	2.6464	10.5041	10^5
46	38+8	2.6667	10.6711	10^5
47	38+9	2.6881	10.8376	10^5
48	39+9	2.7078	11.0029	10^5
54	42+12	2.8254	11.9737	10^5
60	48+12	2.9335	12.9085	10^5
61	48+12+1	2.9511	13.0611	10^5
62	48+13+1	2.9680	13.2135	10^5
63	48+14+1	2.9849	13.3642	10^5
64	48+15+1	3.0017	13.5146	10^5
65	49+15+1	3.0183	13.6644	10^5
66	50+15+1	3.0345	13.8128	10^5
80	58+20+2	3.2479	15.8244	10^5
96	67+25+4	3.4625	17.9833	10^5
100	69+27+4	3.5123	18.5035	10^6
115	78+31+6	3.6876	20.3963	10^5

TABLE I. *(Continued).*

N	Structure	$R_{\rm rms}$	ε	Γ
125	82+35+8	3.7958	21.6132	10^5
128	84+37+7	3.8273	21.9726	10^5
132	85+39+8	3.8683	22.4456	10^5
144	93+41+10	3.9865	23.8383	10^5
146	93+41+12	4.0054	24.0668	10^6
147	93+41+12+1	4.0150	24.1807	10^6
160	100+46+13+1	4.1342	25.6373	10^5
192	114+59+18+1	4.4016	29.0651	10^6
224	128+67+25+4	4.6409	32.3067	10^6
256	142+75+32+7	4.8578	35.3969	10^6
288	156+86+37+9	5.0571	38.3607	10^6
305	163+92+40+10	5.1569	39.8904	10^7
308	163+93+42+10	5.7404	40.1573	10^7
309	163+90+43+12+1	5.1799	40.2460	10^6
320	172+93+42+12+1	5.2419	41.2166	10^6
350	181+105+49+14+1	5.4042	43.8084	10^6
384	195+113+56+19+1	5.5774	46.6582	10^6
448	215+132+70+26+5	5.8768	51.8042	10^6
512	239+146+84+35+8	6.1487	56.7100	10^6
561	255+161+93+42+10	6.3418	60.3288	10^6
565	256+160+93+43+12+1	6.3570	60.6189	10^7
570	257+161+96+43+12+1	6.3760	60.9814	10^7
585	260+168+96+47+13+1	6.4324	62.0623	10^6
634	277+181+106+53+16+1	6.6097	65.5302	10^6
640	278+181+110+54+16+1	6.6308	65.9488	10^6
768	318+211+133+72+29+5	7.0516	74.5869	10^6
888	355+238+158+89+39+9	7.4052	82.2570	10^7
900	356+247+154+92+38+12+1	7.4389	83.0047	10^6
923	361+253+160+93+43+12+1	7.5023	84.4277	10^7
1024	390+275+108+111+53+16+1	7.7696	90.5438	10^6
1200	448+309+212+132+70+25+4	8.1952	100.7410	10^6
1370	482+354+245+155+91+35+8	8.5683	110.1259	10^6
1415	491+365+244+163+94+44+13+1	8.6619	112.5436	10^7
1600	538+398+285+185+115+58+19+2	9.0270	122.2270	10^6
2000	633+470+357+246+163+85+40+6	9.7287	141.1975	10^6
2057	641+491+363+257+158+93+44+10	9.8209	144.6764	10^8
2837	805+634+480+356+246+173+*143*[b]	10.9384	179.4717	10^7
2869	808+644+482+361+249+165+*160*[b]	10.9796	180.8258	10^8
3816	986+793+618+481+*938*[b]	12.0798	218.8847	10^7
3871	992+801+639+*1439*[b]	12.1379	220.9917	10^8
5000	1183+980+802+*2035*[b]	13.2229	262.2696	10^9

[a]Exact static calculation.

[b]The remaining shells cannot be resolved.

parts of the Coulomb interaction. It is well known that systems with short-range interactions arrange themselves in fcc or hcp lattices with coordinations (the number of equal nearest-neighbor distances) of 12 but with higher Madelung energies. A finite Coulomb system, hence, will arrange itself in such a way as to maximize the coordination, i.e., to achieve the maximum possible number of equilateral triangles. The eight-particle configuration, for instance, is not the cube where each particle has *three* nearest neighbors at the same distance but a cube whose upper plane is twisted by 45° with respect to the lower one so that that there are *four* nearest neighbors [17]. In Fig. 1 is shown the front hemisphere of the outer shell of the 5000-particle system. Here the overall hexagonal structure is well pronounced, however, with dislocations and point defects (one particle is missing just below the center, thus making room for a pentagonal structure). The ions on the three outer shells of the same system are shown in Fig. 2. Here the particles in the next inner shell most often are positioned below the line connecting two particles rather than below the center of the triangle. This suggests the following simple geometrical model.

TABLE II. Last subshell and closed-shell particle numbers of multilayer icosahedra.

Shell	Subshell N	Total N
0	1	1
1	12	13
2	42	55
3	92	147
4	162	309
5	252	561
6	362	923
7	492	1415
8	642	2057
9	812	2869
10	1002	3871
11	1212	5083
12	1442	6525

III. GEOMETRICAL MODEL

Denoting the minimal interparticle distance by a, in an ideal hexagonal lattice on a shell an ion occupies an area of twice the area of an equilateral triangle with side a,

$$f = \frac{\sqrt{3}}{2} a^2 . \tag{9}$$

As suggested by the MD results we assume that the next inner and outer shells are shifted by $a/2$ in an arbitrary lattice direction with respect to the reference shell, thereby disregarding curvature effects. Furthermore, the nearest intershell interparticle distances are also a and the ions also form equilateral triangles with sides a if viewed across the shells. This lattice, hence, has two hexagonal surfaces and a square one, and the unit parallelepiped has basis vectors

$$\begin{aligned} \mathbf{a} &= a(1,0,0) , \\ \mathbf{b} &= a(\tfrac{1}{2}, \tfrac{\sqrt{3}}{2}, 0) , \\ \mathbf{c} &= a(\tfrac{1}{2}, 0, \tfrac{\sqrt{3}}{2}) . \end{aligned} \tag{10}$$

The unit areas occupied by one particle normal to the $\mathbf{c}$ and $\mathbf{b}$ directions are equal, $f = ab_y = ac_z$, and the unit volume is $v = ab_y c_z = 3a^3/4$, which, by definition of the Wigner-Seitz radius (4), is equal to $4\pi/3$. The minimum distance, hence, becomes

$$a = \left(\frac{16\pi}{9}\right)^{1/3} = 1.7742 \tag{11}$$

and the intershell distance is

$$d = \frac{\sqrt{3}}{2} a = 1.5365 . \tag{12}$$

These geometrical values are the same as in the cylindrical case [9], where the structures were assumed to consist of helices. The coordination here is 10 (six intrashell and four intershell or vice versa). This lattice is shown in Fig. 3.

On the other hand, a bcc system has the smallest interparticle distance $\sqrt{3}\,c/2$, where $c = (3/2)^{1/3} a$ is the unit distance of the cube with the same density as the hexagonal system. This would give the bcc intershell distance

$$d_{\mathrm{bcc}} = \frac{c}{\sqrt{2}} = 1.4361 . \tag{13}$$

However, in a bcc system the triangles are not equilateral. From Fig. 4 it can be seen that neither limit

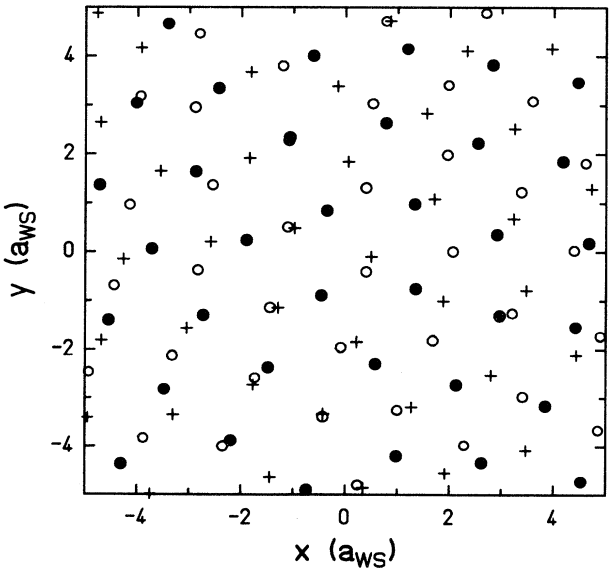

FIG. 2. Close view at the center of Fig. 1 with three outer shells (•, outer shell; +, second outer shell; o, third outer shell).

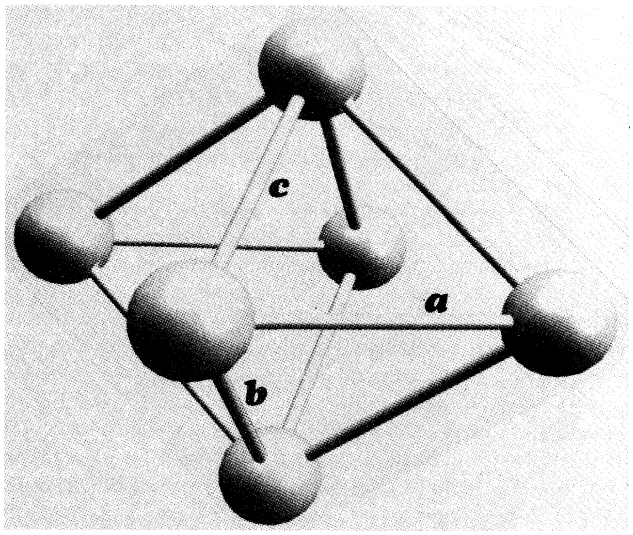

FIG. 3. CAD view into the unit cell of the geometrical model.

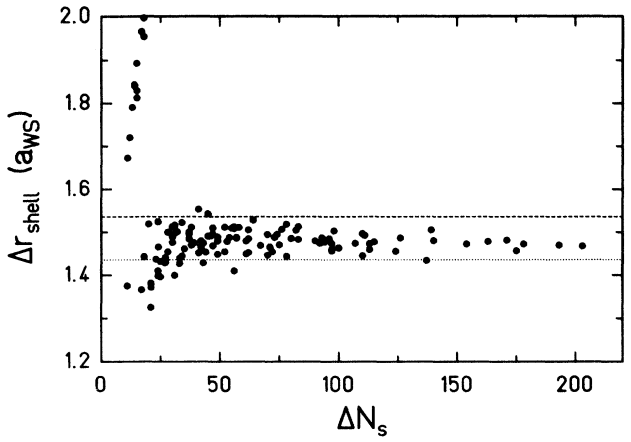

FIG. 4. Difference of shell radii plotted vs the difference of the occupation numbers of these shells. The upper line is the hexagonal geometric limit of Eq. (12) and the lower line is the bcc limit of Eq. (13).

is approached for large systems, the experimental value being $d_{MD} \approx 1.485$. This is mainly due to the fact that there remain dislocations and deviations from the hexagonal structure on and between the shells because of curvature effects. The smallest interparticle distance, Eq. (11), is well reproduced in the MD calculations, as well as the first peaks of the three-dimensional (3D) correlation function of the plane hexagonal lattice at distances a, $\sqrt{3}a$, $2a$, $\sqrt{7}a, \ldots$, see Fig. 5. The intershell correlations at $\sqrt{3/2}\,a$ are strongly suppressed due to the relatively small radial dimensions. There is only little resemblance to the bcc system.

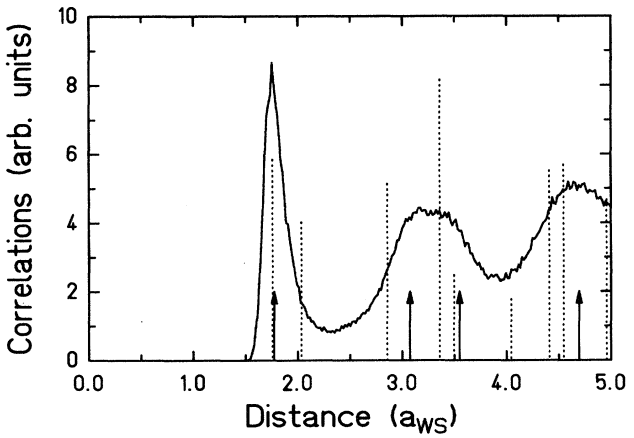

FIG. 5. 3D correlation function (in arbitrary units) of the 5000-ion MD system compared to the correlation function of the bcc lattice (dotted lines). The MD peaks are well situated at those of the plane hexagonal lattice (arrows).

IV. HOMOGENEOUS SYSTEM

The equivalent homogeneous system of radius $\overline{R}$ has Coulomb and confining energies

$$\overline{\varepsilon}_{\rm Coul} = \frac{3}{5}\frac{N}{\overline{R}} , \tag{14}$$

$$\overline{\varepsilon}_{\rm conf} = \frac{1}{2}\overline{R}^2_{\rm rms} = \frac{3}{10}\overline{R}^2 . \tag{15}$$

Minimization with respect to $\overline{R}$ gives

$$\overline{R} = N^{1/3} \tag{16}$$

and the total energy becomes

$$\overline{\varepsilon}_{\rm total} = \frac{9}{10}N^{2/3} . \tag{17}$$

Note that $\overline{\varepsilon}_{\rm Coul} = 2\overline{\varepsilon}_{\rm conf}$ and that this energy per particle is stable to the order N^0 for variations of the radius $\delta\overline{R} \propto N^{-1/3}$. Since the difference in radius between the MD data and the homogeneous value is at least of this order, it suffices to subtract from the MD energies the homogeneous energy in order to simulate the oppositely charged background of an infinite OCP. In the following we subtract these homogeneous values from the total energies and take the difference as excess or Madelung energy.

V. ONION-SHELL MODEL

In order to explain the results of the computer simulations we compare them with those of an onion-shell model, where the crystals are supposed to consist of M homogeneously charged shells of radius R_ν and number of particles N_ν, with the constraint $\sum_\nu N_\nu = N$. The Coulomb and confining energies then become

$$\varepsilon_{\rm Coul} = \frac{1}{N}\left[\sum_{\nu=1}^{M}\frac{N_\nu}{R_\nu}\left(\frac{1}{2}N_\nu + \sum_{\mu(>\nu)}N_\mu\right)\right] , \tag{18}$$

$$\varepsilon_{\rm conf} = \frac{1}{2N}\sum_\nu N_\nu R_\nu^2 . \tag{19}$$

This is corrected for the energy per particle of the plane hexagonal lattice [11, 18],

$$\varepsilon^{\text{pl-hex}}_{\rm Mad} = -\frac{\alpha}{\sqrt{f}} , \tag{20}$$

where $\alpha = 1.960\,515\,789$ and f is the unit area of an ion. This number has been checked by calculating it with the method of Ref. [23],

$$\varepsilon^{\rm 2D}_{\rm Mad} = \frac{1}{a}\left[\gamma - \ln\left(4\pi\frac{a}{b_y}\right) + 4\sum_{m,n=1}^{\infty}K_0\left(2\pi mn\frac{b_y}{a}\right)\cos\left(2\pi mn\frac{b_x}{a}\right)\right] , \tag{21}$$

where γ is Euler's constant, K_0 is the modified Bessel

function, and b_x, b_y are the components of the basis vectors of Eq. (10). Equation (21) converges rapidly after a few terms. With the geometrical value of d, Eq. (20) takes on the value $\varepsilon_{\text{Mad}}^{\text{pl-hex}} = -1.187\,397$. A generalization of the method developed in Ref. [23] allows us to calculate the second-order correction to Eq. (21) due to finite curvature $2/R$,

$$\Delta\varepsilon_{\text{Mad}}^{\text{2D}} = \frac{1}{a}\left(\frac{2a}{R}\right)^2 \frac{\pi}{3}\left(\frac{b_y}{a}\right)^3 \sum_{m,n=1}^{\infty} mn^3 K_1\left(2\pi mn\frac{b_y}{a}\right) \times \cos\left(2\pi mn\frac{b_x}{a}\right) . \tag{22}$$

This has the value $-0.0116N^{-2/3}$ and, thus, is negligible even for small systems.

Minimization of the total energy with respect to the radii yields

$$R_\nu^3 = \frac{1}{2}N_\nu + \sum_{\mu(<\nu)} N_\mu , \tag{23}$$

which in turn gives the total energy per particle

$$\varepsilon_{\text{total}} = \frac{3}{2N}\sum_\nu N_\nu R_\nu^2 + \varepsilon_{\text{Mad}}^{\text{pl-hex}} . \tag{24}$$

Because the lattice structure of the shell surfaces here has only been taken into account globally a minimization with respect to N_ν of Eqs. (23) and (24), such as has been done in Ref. [11] for the cylindrical system, would give an unrealistic recursion relation for the occupation numbers and radii that converge towards the homogeneous radius. This is not in agreement with the MD results of the approximately constant intershell spacing.

We therefore combine the geometric model with the shell model and demand that the area of a given shell be occupied by N_ν areas of equilateral triangles of sides a, thus also allowing for noninteger particle numbers N, N_ν,

$$4\pi R_\nu^2 = \frac{4\pi}{3d}N_\nu + \frac{5}{24}a^2 \qquad (\nu > 0) , \tag{25}$$

where the first term comes from Eq. (9) and the second one is a correction due to finite curvature calculated with spherical geometry. This has been added in order to also yield good results for small particle numbers. Equations (23) and (25) are solved iteratively with initial values $N_0 = R_0 = 0$ to give the results of Table III. The excess energies without $\varepsilon_{\text{Mad}}^{\text{pl-hex}}$ corrections, of course, here would be positive, i.e., higher than the true minimum of the homogeneous system. The agreement of the shell model results with the MD results is rather good, even for the first shell. The opening of new shells is accurately predicted for parts of a particle number and the radii and energies are well reproduced, see Table I.

The Madelung energy of the 3D hexagonal lattice of the geometrical model can be calculated with the general expression [24] for monatomic lattices

$$\varepsilon_{\text{Mad}}^{\text{3D}} = \varepsilon_{\text{Mad}}^{\text{2D}} + \frac{\pi c_z}{ab_y}\left(\frac{1}{6} + 2\sum_{\mathbf{q}\ (\neq\mathbf{0})} \frac{e^{-c_z q}}{c_z q}\frac{\cos\mathbf{c}\cdot\mathbf{q} - e^{-c_z q}}{1 - 2e^{-c_z q}\cos\mathbf{c}\cdot\mathbf{q} + e^{-2c_z q}}\right) , \tag{26}$$

TABLE III. Shell model occupation numbers, radii, and energies per particle.

M	N	N_s	R	R_{rms}	ε	$\varepsilon_{\text{excess}}$
1	13.2	13.2	1.8747	1.8747	5.2719	-0.936670
2	61.8	48.6	3.3465	3.0919	14.3399	-0.912238
3	167.6	105.8	4.8582	4.2924	27.6370	-0.903548
4	352.3	184.7	6.3817	5.4881	45.1780	-0.899507
5	637.7	285.4	7.9103	6.6816	66.9666	-0.897306
6	1045.5	407.9	9.4414	7.8742	93.0037	-0.895976
7	1597.6	552.1	10.9740	9.0661	123.2899	-0.895113
8	2315.8	718.1	12.5076	10.2575	157.8255	-0.894520
9	3221.6	905.9	14.0419	11.4487	196.6104	-0.894096
10	4337.0	1115.4	15.5765	12.6398	239.6449	-0.893782
11	5683.7	1346.7	17.1115	13.8306	286.9290	-0.893543
12	7283.4	1599.7	18.6468	15.0214	338.4626	-0.893357
13	9158.0	1874.6	20.1823	16.2120	394.2458	-0.893209
14	11329.2	2171.2	21.7179	17.4027	454.2787	-0.893090
15	13818.7	2489.5	23.2536	18.5932	518.5611	-0.892992
20	31803.4	4407.8	30.9334	24.5454	903.7177	-0.892695
50	470634.1	27344.3	77.0241	60.2534	5445.7157	-0.892353
100	3696059.8	109103.0	153.8487	119.7636	21514.9890	-0.892301
200	29294081.9	435862.3	307.5004	238.7828	85525.8245	-0.892288
500	455155840.8	2722075.7	768.4575	595.8393	532536.6438	-0.892284
999	3623534378.3	10863792.3	1535.1835	1189.7429	2123232.2095	-0.892283

with the first term given by Eq. (21). Here, $\mathbf{q} = k_a\mathbf{a}^* + k_b\mathbf{b}^*$, k_a, k_b take on integer values and

$$\mathbf{a}^* = \left(\frac{2\pi}{a}, -\frac{2\pi b_x}{ab_y}, 0\right) ,$$
$$\mathbf{b}^* = \left(0, \frac{2\pi}{b_y}, 0\right) \tag{27}$$

are the reciprocal-lattice vectors. Within an accuracy of 10^{-5} we can restrict the summation over $\mathbf{q}$ in Eq. (27) over the smallest six reciprocal-lattice vectors with $c_z q = 2\pi$. The second term of Eq. (26) is the energy of the background charge and has the value $d^2/8 = 0.295\,114$; and the third term, $-0.002\,100$, is the energy of the lattice-lattice interactions. This yields

$$\varepsilon_{\mathrm{Mad}}^{\text{3-hex}} = -0.894\,383 , \tag{28}$$

above the bcc ($-0.895\,929$), fcc ($-0.895\,874$) and hcp ($-0.895\,838$) values but below the MD result ($-0.892\,80$), see Fig. 6, and of the sc lattice ($-0.880\,059$).

VI. ASYMPTOTIC FORMS

For very large particle numbers the system of equations [(23),(25)] converges towards equidistant concentric shells with shell spacing d and excess energy

$$\varepsilon_{\mathrm{Mad}}^{\text{model}} = \varepsilon_{\mathrm{Mad}}^{\text{pl-hex}} + \frac{d^2}{8} = -0.892\,283 . \tag{29}$$

Here the second term is identical to the second term of Eq. (26). However, as can be seen from Table III, up to this accuracy this limit is reached only for 10^6 particles.

The excess (or Madelung) energies are compared in Fig. 6 with the MD results. Here the best fit for $N > 300$ gives

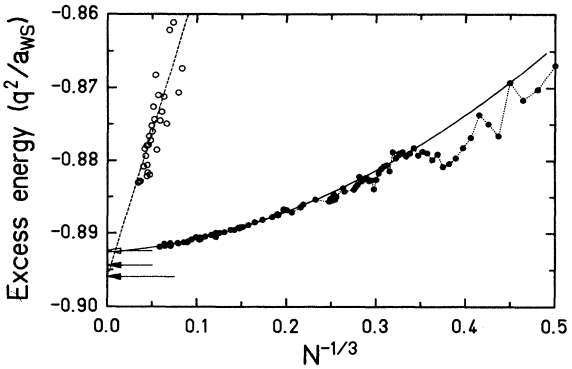

FIG. 6. Excess (Madelung) energy per particle in units of q^2/a_{WS} vs $N^{-1/3}$. The dots are molecular-dynamics data and the dotted line is to guide the eye. The full line is the best fit for $N > 300$. The open arrow points to the result of the shell model including a correction for plane haxagonal surfaces, the full arrow is the Madelung energy of the infinite 3D lattice of the geometrical model, and the long arrow is the Madelung energy of the infinite bcc OCP. Open circles are results of fragments of spherical bcc matter with up to 25 000 particles together with a fit (dashed line).

$$\varepsilon_{\mathrm{MD}} = -0.8926 \pm 0.0001 + 0.0088N^{-1/3} + 0.096N^{-2/3} , \tag{30}$$

where the error is estimated from fits to $N > 200$ and $N > 500$, respectively. For systems with $N < 64$, there are strong shell effects in the excess energy with peaks, and minima if a new shell opens, in particular the transitions at $N = 12, 60, 146$. These shell effects, however, are about four times smaller than in the cylindrical case [16].

Large systems then exhibit rather well an $N^{-1/3}$ systematics of the surface-energy correction. The shell model corresponds to smearing the ion charge over one shell or, in other words, only using $\mathbf{q} = \mathbf{0}$ in Eq. (26). The shell model, thus, does not give a correction to the excess energy, which goes like $N^{-1/3}$. Here the *surface* term is missing and the *curvature* correction is proportional to $N^{-2/3}$. Equation (26) sums up all interactions of a particular ion with those in the inner and outer layers. Ions in the surface layer, however, have only an inner neighboring shell. The surface correction to Eq. (26) can therefore be estimated from the missing contributions of terms with $\mathbf{q} \neq \mathbf{0}$. According to Ref. [24] this energy per ion is

$$\frac{\pi c_z}{ab_y} \sum_{\mathbf{q}\ (\neq \mathbf{0})} \frac{\mathrm{e}^{-c_z q}}{c_z q} \cos \mathbf{c}\cdot\mathbf{q} . \tag{31}$$

For two neighboring ionic layers this contribution therefore becomes $\mathrm{e}^{-2\pi}/a$ per surface ion. The number of surface ions is $4\pi R^2/ab_y = 3c_z N^{2/3}$ and, hence, the surface correction per particle becomes approximately

$$\Delta\varepsilon_{\mathrm{Mad}}^{\mathrm{3D}} = \frac{3c_z}{a}\,\mathrm{e}^{-2\pi}\,N^{-1/3} , \tag{32}$$

which takes on the value $0.004\,85N^{-1/3}$. Higher contributions from larger reciprocal-lattice vectors within a layer go like $\mathrm{e}^{-2\sqrt{3}\pi}$, $\mathrm{e}^{-4\pi}, \ldots$, and those across more than one shell like $\mathrm{e}^{-4\pi}, \ldots$. Other higher-order terms also arise from unevenly spaced shells [18]. These effects of surface relaxation change the value of c_z, and their contributions are differences of the terms (32) with slightly different values of c_z. One can describe this process as the response of the harmonic crystal to an external force proportional to $\mathrm{e}^{-2\pi}$, and in this case the change of energy is proportional to $\mathrm{e}^{-4\pi}$. All these higher-order terms are neglected, as they are smaller by at least two orders of magnitude.

Alternatively, one can also vary the plane unit area f with respect to d under the constraint of constant unit volume, and minimize the excess energy $d^2/8 - \alpha/\sqrt{f}$ with $f = 4\pi/3d$ with respect to d, as has been done in Refs. [18, 16]. This gives

$$d_{\mathrm{m}} = \left(\frac{3\alpha^2}{\pi}\right)^{1/3} = 1.5425 \tag{33}$$

and the minimized excess energy becomes

$$-\frac{3}{8}d_{\mathrm{m}}^2 = -0.892\,290 , \tag{34}$$

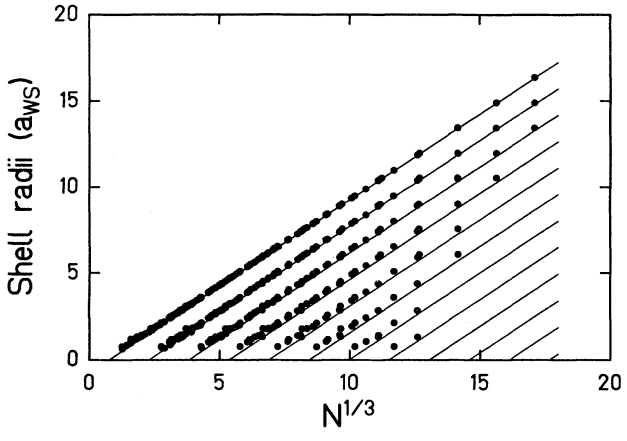

FIG. 7. MD shell radii vs $N^{1/3}$ compared to the shell model result of Eq. (35).

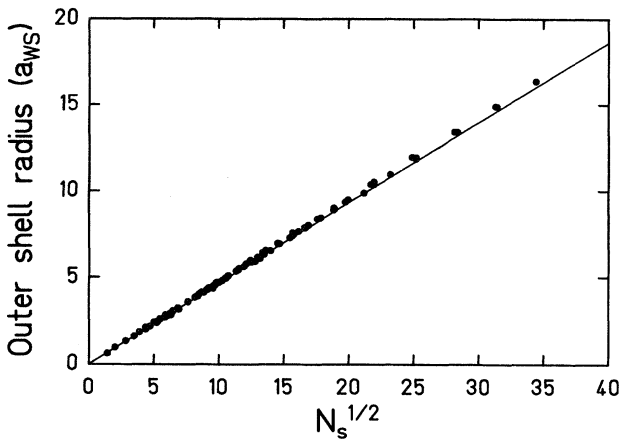

FIG. 9. MD outer shell radius vs the square root of the number of particles in this shell compared to the shell model result of Eq. (35).

in close agreement with the geometrical, shell model, and MD values. In any case, these Madelung energies are much higher than the Madelung energy of the infinite bcc OCP of $-0.895\,929$.

In addition, for $N \gg 1$, in the shell model the shells become equidistant with d, thus $R_\nu = \nu d$. With Eq. (23) and the particle number conservation this gives three relations connecting R_ν, N_ν, and N,

$$R_\mu = \sqrt{N_\mu/3d} = N^{1/3} - (\mu + \tfrac{1}{2})d \,. \tag{35}$$

Here, $\mu = 0, 1, \ldots, M$ counts the shells from the outside. The number of shells then becomes

$$M = \frac{1}{d}N^{1/3} - \frac{1}{2} \,. \tag{36}$$

These relations are compared in Figs. 7–9 with the MD results. The number of shells is well predicted (e.g., 11 shells for $N = 5000$), but, due to the difference in d and d_{MD}, there remain small discrepancies in the slopes of the theoretical results. Note that, although the multilayer icosahedra cannot be realized exactly as Coulomb crystals because they are far from being spherical and the influence of the pentagonal substructures is too strong, the closed-shell ion numbers are well attained. Bringing Eq. (8) into the form of Eq. (36) would give an intershell spacing of $d_{\mathrm{MLI}} = (10/3)^{1/3} = 1.4938$ even closer to the experimental MD value.

As a final test of the model the rms radius is calculated to second order. In order to maintain the relation $\varepsilon_{\mathrm{Coul}} = 2\varepsilon_{\mathrm{conf}}$ the confining energy is one-third of the total energy, which, in turn is $\frac{1}{2}R_{\mathrm{rms}}^2$. From this the rms radius becomes

$$R_{\mathrm{rms}} = \sqrt{\frac{3}{5}}N^{1/3} - \sqrt{\frac{5}{3}}\,\frac{\varepsilon_{\mathrm{Mad}}^{\mathrm{model}}}{3}N^{-1/3} \,. \tag{37}$$

The excess of this rms radius, i.e., the second term of Eq. (37) (the first term is the homogeneous part), is compared in Fig. 10 with the MD results. For large N there is perfect agreement.

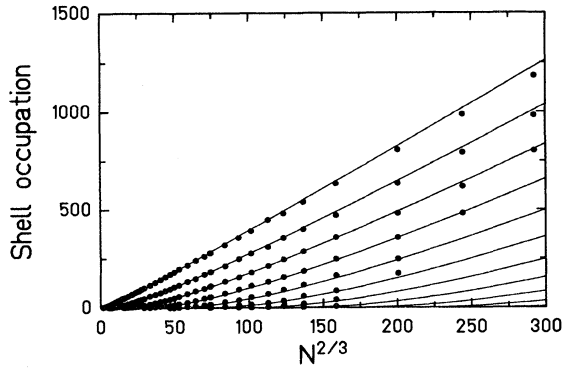

FIG. 8. MD occupation numbers of the different shells vs $N^{2/3}$ compared to the shell model result of Eq. (35).

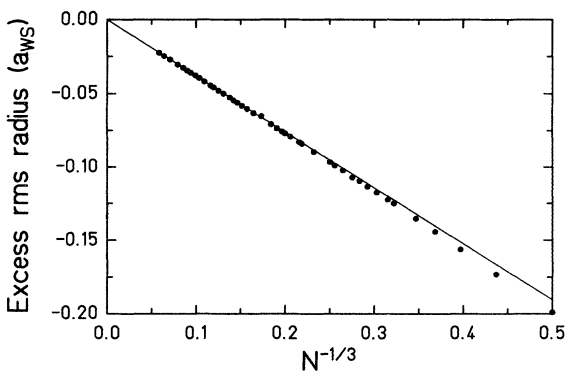

FIG. 10. MD excess rms radius vs $N^{-1/3}$ compared to the shell model result of Eq. (37).

VII. SUMMARY AND DISCUSSION

We have performed molecular-dynamics computer simulations of spherical crystals under the influence of a harmonic confining force and of the interparticle Coulomb forces. Systems of 2 to 5000 particles were calculated at very low kinetic energy. The resulting interparticle distances, radii, occupation numbers, and Madelung energies were compared with theoretical results by combining a geometric model where the unit cell consists of two shifted parallel planes of equilateral triangles and an onion-shell model where the surfaces are homogeneously charged. The theoretical and experimental Madelung (excess) energies are in close agreement but higher than the bcc value, thus indicating that even at such large particle numbers the *hexagonal* surface structure still dominates the bcc structure. The particle numbers at shell closure and the number of shells are also in very good agreement with those obtained from multilayer icosahedra.

The small surface-energy term is a peculiarity of the hexagonal (001) geometrical lattice. Other systems whose structures are not closed packed have much higher surface energies [12]. The surface energy (30) extracted from the MD data is the average over the whole surface and also includes relaxation and reconstruction of the surface that minimize the total energy. To evaluate the order of magnitude of surface relaxation we calculated the excess energies of unrelaxed spherical fragments containing up to 25 000 particles, sliced out of infinite ideal bcc matter with the same density; see the open circles in Fig. 6. Extrapolation of these data to the bcc Madelung energy (dashed line) gives a surface-energy coefficient of ≈ 0.4. It crosses the fit of the MD data at $N \approx 4 \times 10^6$. This number of particles at which the infinite bcc lattice takes over energetically is compatible with the estimate of Dubin [12].

ACKNOWLEDGMENTS

One of us (R.W.H.) acknowledges fruitful discussions with S. Ichimaru and J.P. Schiffer. He also thanks R. Schmidt for bringing to his attention the theory of multilayer icosahedra. The other (V.V.A.) thanks the ESR division of GSI Darmstadt for the kind hospitality extended to him.

[1] R.F. Wuerker, H. Shelton, and R.V. Langmuir, J. Appl. Phys. **30**, 342 (1959).
[2] P.E. Toschek, Phys. Blätt. **45**, 465 (1989).
[3] F. Diedrich, E. Peik, J.M. Chen, W. Quint, and H. Walther, Phys. Rev. Lett. **59**, 2931 (1987).
[4] D.J. Wineland, J.C. Bergquist, W.M. Itano, J.J. Bollinger, and C.H. Manney, Phys. Rev. Lett. **59**, 2953 (1987).
[5] S.L. Gilbert, J.J. Bollinger, and D.J. Wineland, Phys. Rev. Lett. **60**, 2022 (1988).
[6] S. Ichimaru, Rev. Mod. Phys. **54**, 1017 (1982).
[7] J.J. Thomson, Philos. Mag. **39**, 237 (1904); **41**, 510 (1921).
[8] A. Rahman and J.P. Schiffer, Phys. Rev. Lett. **57**, 1133 (1986).
[9] R.W. Hasse and J.P. Schiffer, Ann. Phys. **203**, 419 (1990).
[10] H. Totsuji, Phys. Rev. A **17**, 399 (1978).
[11] H. Totsuji and J.-L. Barrat, Phys. Rev. Lett. **60**, 2484 (1988).
[12] D.H.E. Dubin and T.M. O'Neil, Phys. Rev. Lett. **60**, 511 (1988).
[13] J. Mostowski and M. Gajda, Acta Phys. Pol. A **67**, 783 (1985).
[14] Yu.E. Lozovik and V.A. Mandelstam, Phys. Lett. A **145**, 269 (1990).
[15] J.P. Schiffer, in GSI Report No. 89-10 (1989), p.2.
[16] R.W. Hasse, Phys. Rev. Lett. **67**, 600 (1991).
[17] R. Rafac, J.P. Schiffer, J.S. Hangst, D.H.E. Dubin, and D.J. Wales, Proc. Natl. Acad. Sci. (USA) **88**, 483 (1991).
[18] D.H.E. Dubin, Phys. Rev. A **40**, 1140 (1989).
[19] R. Casdorff and R. Blatt, Appl. Phys. B **45**, 175 (1988).
[20] W. Slattery, G. Doolen, and H. DeWitt, Phys. Rev. A **21**, 2087 (1980).
[21] A.L. Mackay, Acta Crystallogr. **15**, 916 (1962).
[22] S. Bjørnholm, Contemp. Phys. **31**, 309 (1990).
[23] V.V. Avilov, Solid State Commun. **44**, 555 (1982).
[24] V.V. Avilov, Fiz. Tverd. Tela **14**, 2550 (1972) [Sov. Phys.—Solid State **14**, 2209 (1973)].

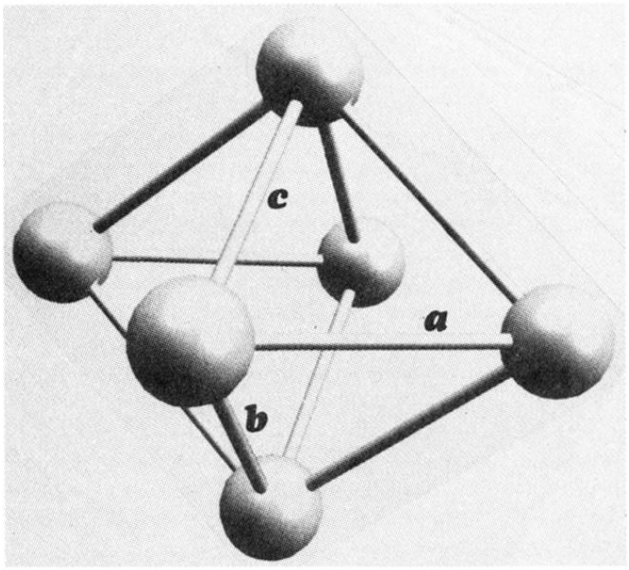

FIG. 3. CAD view into the unit cell of the geometrical model.